

NANO EXPRESS

Open Access



Magnetoviscous Property and Hyperthermia Effect of Amorphous Nanoparticle Aqueous Ferrofluids

Chuncheng Yang^{1,2*}, Mengchun Yu², Shuchun Zhao², Yuan Tian² and Xiufang Bian^{2*}

Abstract

Magnetic Fe-B, Fe-Ni-B, and Co-B nanoparticles were successfully synthesized and introduced to water to prepare aqueous ferrofluids. The Fe-B, Fe-Ni-B, and Co-B particles are homogeneous amorphous nanoparticles with an average particle size 15 nm. The shape of the amorphous nanoparticles is regular. The Fe-B, Fe-Ni-B, and Co-B amorphous nanoparticles are superparamagnetic. Moreover, the saturation magnetizations of Fe-B and Fe-Ni-B amorphous nanoparticles are 75 emu/g and 51 emu/g. These are approximately 2.8 and 1.9-fold larger than Co-B nanoparticles, respectively. The viscosity of the amorphous ferrofluids has a strong response to external magnetic field. The yield stress increases with increasing magnetic field. The hyperthermia research of amorphous ferrofluids was firstly investigated. The experimental results indicate that the heating temperature of Fe-B ferrofluid and Fe-Ni-B ferrofluid could increase to 42 °C in 750 s and 960 s, respectively, when the output current is 300 A. The temperature could reach 61.6 °C for a Fe-B ferrofluid. The heating efficiencies of the amorphous ferrofluids demonstrate that the Fe-B ferrofluid and Fe-Ni-B ferrofluid may have great potential for biomedical applications.

Keywords: Amorphous nanoparticle, Aqueous ferrofluids, Viscosity, Hyperthermia effect

Introduction

Ferrofluids (FFs), also called magnetic fluids, are colloidal solutions of magnetic nanoparticles in a fluid carrier such as organic solvents, water [1–5]. As a new type of smart functional materials, FFs offer unique physical, chemical, and biocompatible properties [6–9]. FFs have been applied in biomedicine for magnetic resonance imaging (MRI) [10] and target drug delivery [11], as well as for phase separation [12], removal of water pollutants [13], and sensing [14].

The increased viscosity induced by the applied magnetic field influences FF applications. Studies on magnetoviscous properties evaluate the viscosity variations in FFs as a function of time, temperature, shear rate, or other factors under applied magnetic fields [4, 15–20]. Rajnak [18] studied the viscosity of a transformer oil-based FF and found that the electric field-induced

viscosity changes are analogous to the magnetoviscous effect. Nowak [19] investigated the changing viscosity of FFs diluted with sheep blood. They found that the strong magnetoviscous effect leads to the assumption of big changes in the microstructure due to magnetic fields. Prior work demonstrated a significant interaction of the carrier medium and surfactant with a consideration of the magnetic behavior of FFs [20]. Research on the magnetoviscous properties of FFs remains a focal point. The amorphous alloys have a promising future for fuel cell electrode [21], nano-porous materials [22], biodegradation materials [23], etc. due to their unique properties related to amorphous metastable atomic structure and low-cost raw materials [24]. Other studies showed that amorphous soft magnetic Fe-based alloys have great potential applications in preparing magnetic functional fluids because of their unique magnetic properties versus crystalline alloys [25]. Fe_{73.5}Nb₃Cu₁Si_{13.5}B₉ [26, 27] and Fe₇₈Si₉B₁₃ amorphous alloy particles have been applied in magnetorheological fluids. However, it is difficult to prepare amorphous nanoparticles applied in

* Correspondence: chunchengyoung@163.com; xfbian@sdu.edu.cn

¹School of Gemology and Materials Technology, Hebei GEO University, Shijiazhuang 050031, China

²Key Laboratory for Liquid-Solid Structural Evolution and Processing of Materials, Ministry of Education, Shandong University, Jinan 250061, China

FFs via a conventional mechanical milling method. Our group synthesized and investigated magnetic Co-Fe-Si-B [28] amorphous nanoparticles as well as Fe-Co-B [29] amorphous nanoparticles applied to FFs. These data show that the amorphous FFs exhibit good stability. Nevertheless, little attention has been given to the magnetoviscous property of FFs based on amorphous nanoparticles.

Hyperthermia therapy has been a focus of cancer treatment, and magnetic fluid hyperthermia (MFH also called FF hyperthermia) is a therapeutic procedure. FFs are injected into tissues containing cancerous cells and then exposed to a frequency alternating magnetic field, resulting in a temperature rise up to 42–45 °C to destroy the tumor cells [30–32]. Importantly, the nanoparticles in the FFs must not be toxic. Iron oxide (Fe_3O_4) or cobalt iron oxide (CoFe_2O_4) nanoparticles are popularly selected to prepare FFs for magnetic fluid hyperthermia because of their simple processing, low cost, and good biological compatibility [33–38]. Lahiri [38] studied the alternating magnetic field-induced heating of a water-based FF using infrared thermography. The FF contains tetramethyl ammonium hydroxide-coated iron oxide nanoparticles. The results indicate a higher initial rate of temperature rise and a lower maximum temperature at the end of the heating period. Zubarev [39] reported the effect of magnetic interactions between single domain ferromagnetic particles on the hyperthermia effect produced by these particles under the action of an oscillating magnetic field. However, few studies have reported hyperthermia research on amorphous magnetic nanoparticle FFs.

In this paper, magnetic Fe-B, Fe-Ni-B, and Co-B amorphous nanoparticles were successfully synthesized by a chemical reduction method. The structure, morphology, and magnetic properties of the amorphous nanoparticles were investigated. The magnetoviscous properties and hyperthermia effect of corresponding FFs were also studied. In view of the magnetic properties and prominent heating effect, the amorphous FFs as promising materials in medical applications could also offer opportunities in emerging areas such as cooling applications, energy conversion devices, printed electronics, etc.

Materials and Methods

Ferrous sulfate ($\text{FeSO}_4 \cdot 7\text{H}_2\text{O}$), cobalt chloride ($\text{CoCl}_2 \cdot 6\text{H}_2\text{O}$), nickel chloride ($\text{NiCl}_2 \cdot 6\text{H}_2\text{O}$), sodium borohydride (NaBH_4), sodium hydroxide (NaOH), ethyl alcohol, agar, and polyethylene glycol (PEG-400) were used. All chemicals were of analytical reagent (AR) grade and used without further purification. Before each experiment, all glassware were cleaned with dilute nitric and repeatedly washed with deionized water.

The amorphous particles were prepared by chemical reduction. In a typical process, a solution was obtained by dissolving certain amount of $\text{FeSO}_4 \cdot 7\text{H}_2\text{O}$ and $\text{NiCl}_2 \cdot 6\text{H}_2\text{O}$ into 200 ml of 50% ethanol solution with mechanical stirring and supersonic dispersion. Then, 50 ml of 0.8 M NaBH_4 aqueous solution was added dropwise as a reducing agent at a speed of 1.5 ml/min at 20 °C in a three-necked flask under a protective argon environment. Here, the NaOH solution was used to adjust the pH of NaBH_4 solution to 10–12. After stirring with supersonic dispersion for 2.5 h, the black precipitate was separated using a magnet. The particles were washed with deionized water for several times. After that, appropriate 0.075 g agar was added as the first surfactant and 0.05 g PEG-400 was added as the second surfactant. These were put into the Fe-Ni-B particle suspension at a constant temperature. The mixture was stirred for 1 h at a constant temperature. Finally, the stable Fe-Ni-B amorphous aqueous FF was obtained after cooling to room temperature.

The Fe-B amorphous particles were obtained using a chemical reduction method, i.e., from the reduction of $\text{FeSO}_4 \cdot 7\text{H}_2\text{O}$ using NaBH_4 as a reducing agent in aqueous solution. Co-B amorphous particles were obtained from the reduction of $\text{CoCl}_2 \cdot 6\text{H}_2\text{O}$ solutions. The corresponding Fe-B aqueous FF and Co-B aqueous FF were similarly obtained.

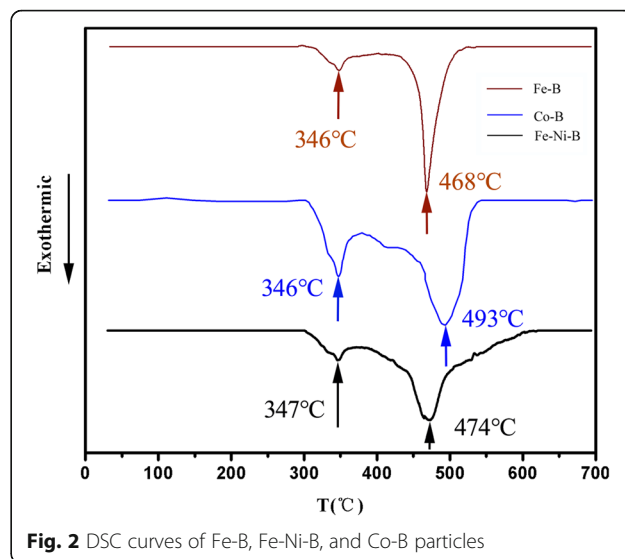
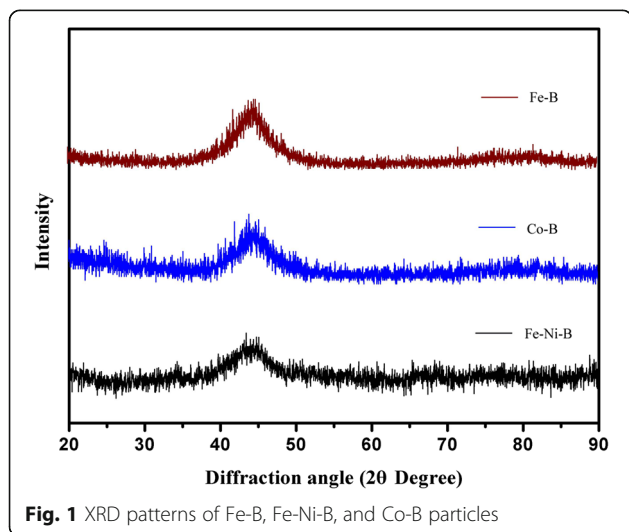
The structure and amorphous state of magnetic Fe-B, Fe-Ni-B, and Co-B amorphous nanoparticles were characterized by X-ray diffraction (XRD) measurements using a D/max-Rb, with a Ni-filtered $\text{Cu K}\alpha$ radiation source. The thermal properties were characterized with a differential scanning calorimeter (Netzsch DSC 404 C) at a heating rate of 20 °C/min. The magnetic properties of the amorphous nanoparticles were measured with an alternating gradient force magnetometer (AGM) at room temperature. The morphologies of the amorphous nanoparticles were identified via transmission electron microscopy (TEM). The magnetoviscous properties of FFs were studied with a rheometer (Anton Paar MCR301) equipped with an external controllable magnetic field. The hyperthermia effects of the amorphous FFs were studied using a device shown in Fig. 8a. Field-induced heating experiments were performed using a radio frequency induction heating system (AtecD, Bamac, China) consisting of a high-frequency generator and a tank circuit equipped with water-cooled electrolytic copper coils. The experiments were performed at a fixed frequency of 90 kHz, and the magnetic field was changed by varying the coil current. An infrared thermometer (OSXL207, Omega, USA) with an accuracy of 0.1 °C was used to record the temperature in the magnetic heating experiment. The error in our temperature measurement is with 1 °C. The experimental tests were performed at room temperature.

Results and Discussion

Figure 1 shows the X-ray diffraction (XRD) patterns of magnetic Fe-B, Fe-Ni-B, and Co-B particles, respectively. The Fe-B, Fe-Ni-B, and Co-B particles consist of a broad single peak in the 2θ range of $40^\circ\sim 50^\circ$ and no crystalline peak can be seen, which is characteristic of amorphous structure (Fig. 1). The results indicate that Fe-B, Fe-Ni-B, and Co-B particles have a typical amorphous structure.

The differential scanning calorimeter (DSC) curves of the Fe-B, Fe-Ni-B, and Co-B particles are shown in Fig. 2. The experiments were carried out at a heating rate of $20^\circ\text{C}/\text{min}$. Fe-B, Fe-Ni-B, and Co-B particles exhibit two exothermic peaks demonstrating two-stage crystallization processes [40]. The temperatures of two exothermic peaks are marked in Fig. 2, which could help select the annealing temperature of the amorphous particles in subsequent work. These results correspond well with the XRD data.

The magnetic properties of the as-prepared Fe-B, Fe-Ni-B, and Co-B particles were characterized by AGM at room temperature. The magnetic hysteresis curves are shown in Fig. 3. The saturation magnetizations (M_s) of the Fe-B particles and Fe-Ni-B particles are 75 emu/g and 51 emu/g, respectively. Moreover, no coercivity and remanence are observed on the hysteresis curves, confirming the superparamagnetism of the Fe-B and Fe-Ni-B particles. The M_s of the Co-B particles is 27 emu/g; these particles also exhibit superparamagnetic behavior. In addition, the M_s of Fe-B and Fe-Ni-B particles are approximately 2.8- and 1.9-fold larger than the Co-B particles, respectively. Also we can see that the M_s of the Fe-B particles is higher than that of Fe_3O_4 particles and CoFe_2O_4 particles [26]. The structure, size, magnetization, and concentration of different FF samples can be seen in Table 1.



We next investigated the morphologies of the amorphous particles in FFs with TEM (Fig. 4). The FFs were diluted and then dispersed in an ultrasonic for 20 min. The support films adhered with a copper net were immersed in diluted FFs. The specimens were prepared well after drying the sample in an oven for 30 min. The TEM images shown in Fig. 4 demonstrate that the amorphous particles in FFs are nearly spherical. The average mean diameters of the amorphous particles are ~ 15 nm.

The magnetoviscous properties of the three amorphous FFs (Fe-B FF, Fe-Ni-B FF, and Co-B FF) with 1.8 wt% of magnetic particles were investigated by a rheometer with an external controllable magnetic field. The viscosity of each sample was measured two times at a constant set temperature 25°C . Every time the sample went through one cycle of shear rate sweep

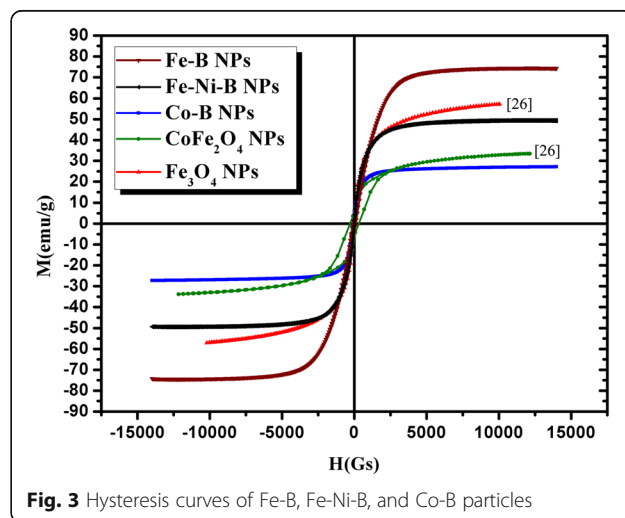


Table 1 The structure, size, magnetization, and concentration of different FF samples

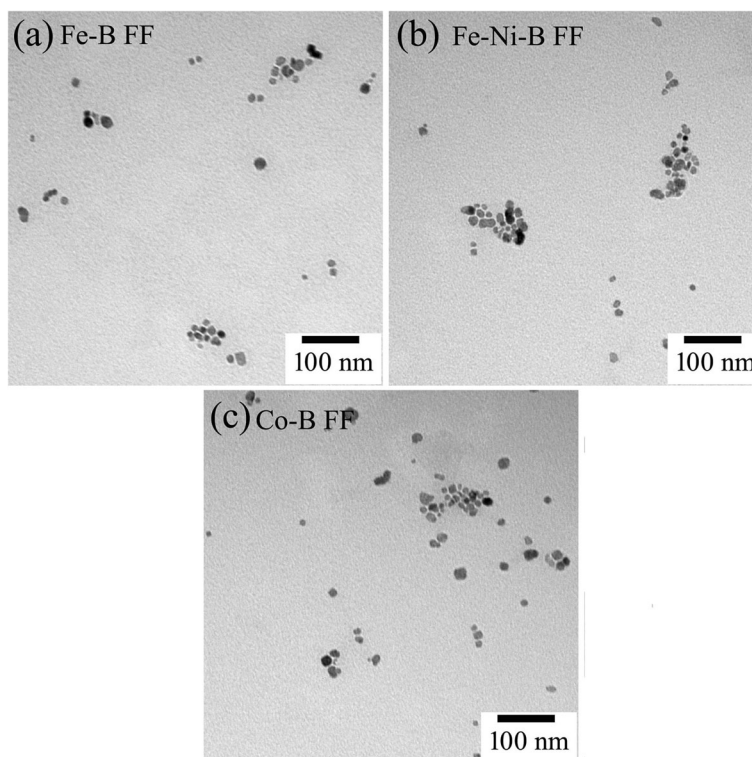
FFs composition	Structure	Physical diameter by TEM (nm)	Magnetization at 14 kOe (emu/g)	Concentration (wt%)
Fe-B	Amorphous	11–14	75	1.8
Fe-Ni-B	Amorphous	12–15	51	1.8
Co-B	Amorphous	13–15	27	1.8

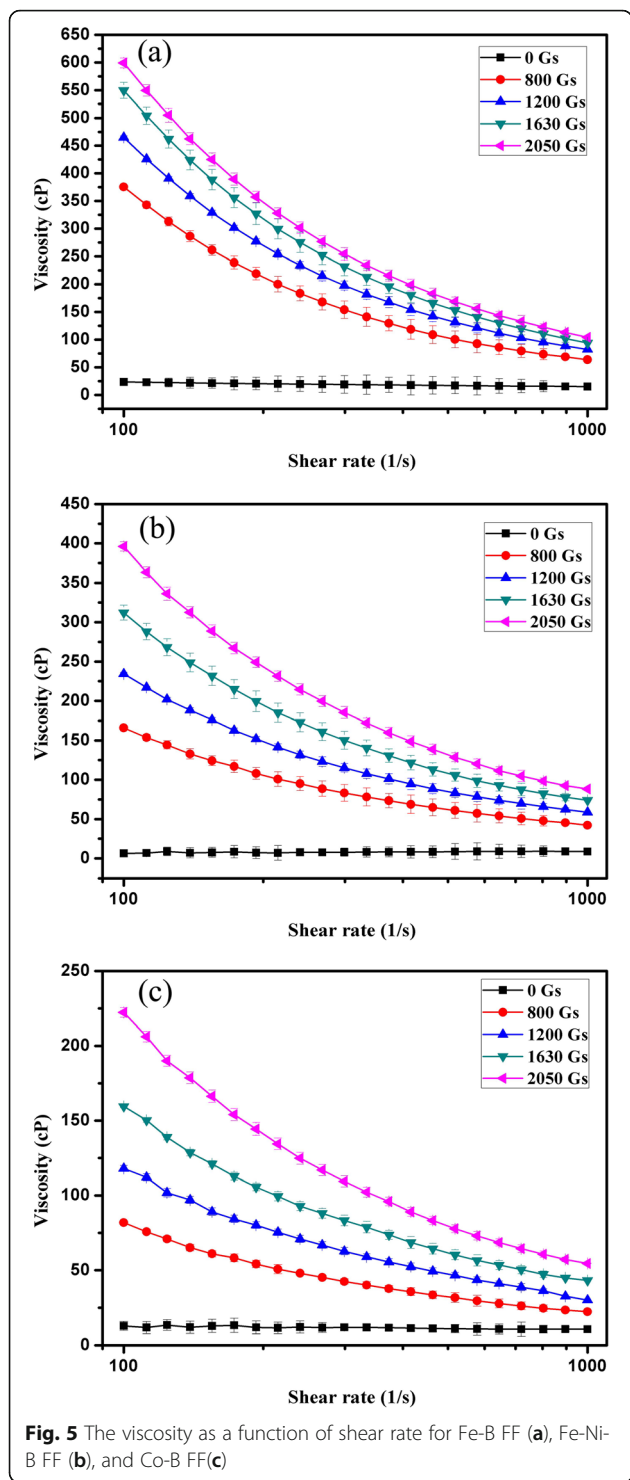
ramping up from 100 to 1000 1/s and then ramping down from 1000 to 100 1/s. The average value was obtained by calculating the viscosity at the same shear rate. The viscosity-shear rate curves of amorphous FFs under different external magnetic fields on a logarithmic scale are shown in Fig. 5. All the amorphous FFs (Fe-B FF in Fig. 5a, Fe-Ni-B FF in Fig. 5b, and Co-B FF in Fig. 5c) exhibit shear thinning behavior under different magnetic fields. The viscosity decreases with increasing shear rates. The Fe-B FF has a larger viscosity than Fe-Ni-B FF and Co-B FF. This is because of the Ms of the amorphous Fe-B nanoparticles, Fe-Ni-B nanoparticles, and Co-B nanoparticles.

The magnetic field also plays an important role in the viscosity of amorphous FFs. The viscosity is shown as a function of magnetic field in Fig. 6. The results demonstrate that the viscosity of all amorphous FFs increase with increasing external magnetic field. This corresponds well

with the results in Fig. 5. The magnetic amorphous nanoparticles in FFs rearranged their orientation when a magnetic field was applied. It aligned in the direction of magnetic field. The interaction and arrangement of the nanoparticles in the FFs became stronger with increasing magnetic field intensity, which led to increased flow resistance. Moreover, prior reports [15, 41–46] show that with increasing magnetic field, chain-like or drop-like structures, and aggregation could form in FFs, which leads to a remarkable increase in viscosity. The observed shear thinning behavior in Fig. 5 could be explained by breaking of these chains or drops due to shear. The nanoparticles begin to arrange their orientation in the shearing direction when the applied shear rate increases. Moreover, the increasing shear rate destroys chains or drop-like aggregates; consequently, the FF viscosity decreases.

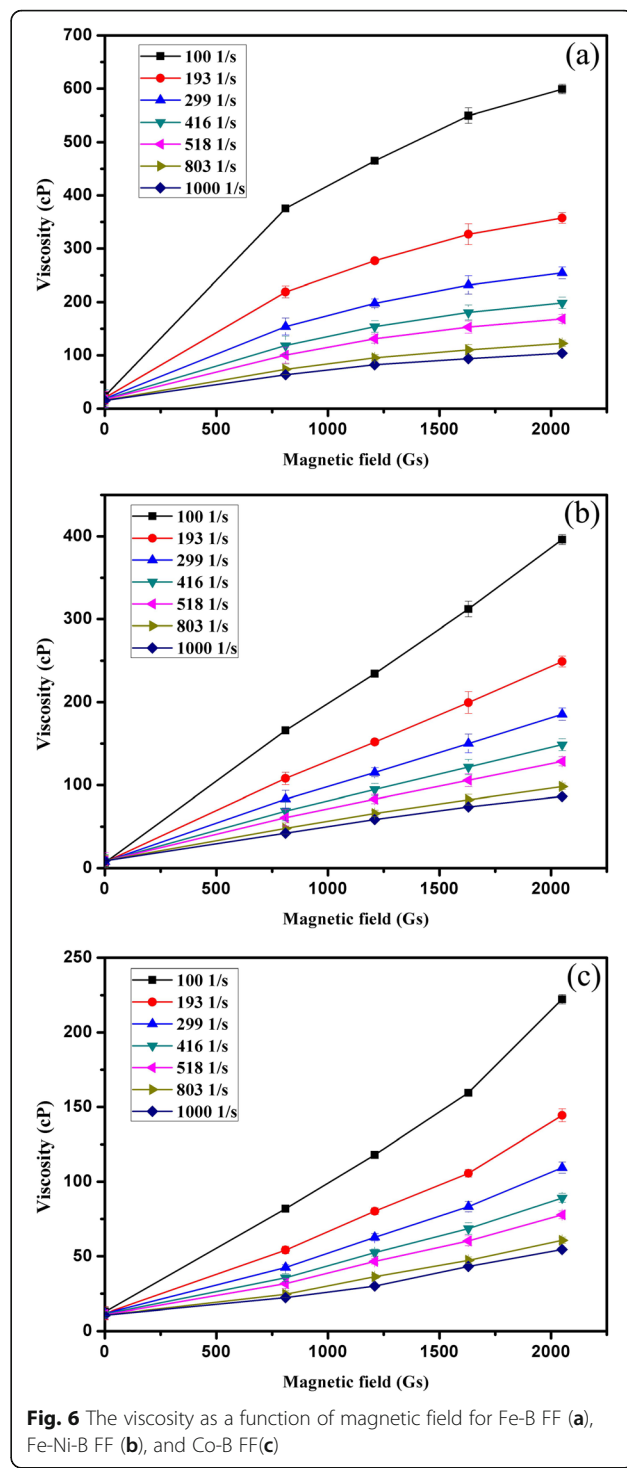
The yield stress of FF can be obtained via linear extrapolation, and the intercept of each fitting curve is considered to be the yield stress of the FF under the corresponding magnetic field [27]. Therefore, the yield stresses of the three amorphous FFs under different magnetic fields are obtained in Fig. 7. It demonstrates that the yield stress of FFs increases with increasing magnetic strength especially for the amorphous Fe-B FF. This is because chain-like or drop-like structures as well as aggregates are formed under the applied magnetic field. The force between amorphous nanoparticles becomes stronger while

**Fig. 4** TEM images of Fe-B FF (a), Fe-Ni-B FF (b), and Co-B FF (c)

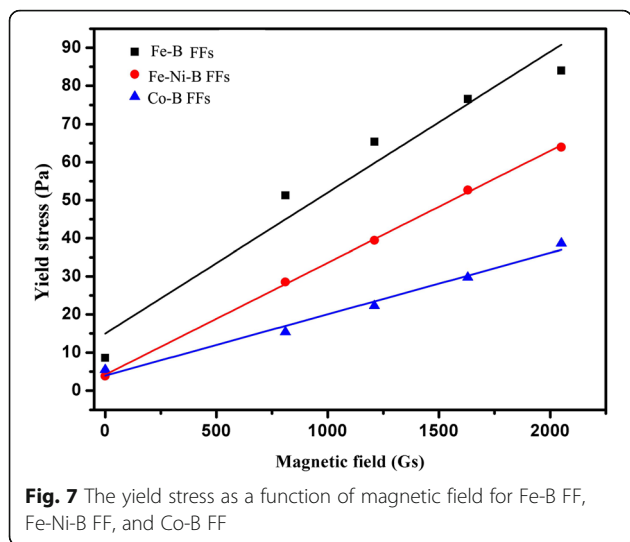


increasing magnetic strength. Prior work [47] showed that the yield stress of amorphous FFs is due to the magnetization of the magnetic amorphous nanoparticles.

FF hyperthermia has attached much importance due to its safety and limited physical or mental strain on



the patients [26, 48–50]. Such hyperthermia is induced by heating effects in an alternating current (AC) magnetic field. We studied the hyperthermia effects of FFs with Fe-based amorphous nanoparticles, i.e., Fe-B FF and Fe-Ni-B FF. A schematic map of the experimental device is shown in Fig. 8a. An IR thermometer with an



accuracy of 0.1 °C recorded the temperature in the magnetic heating experiment. The error in our temperature measurement is 1 °C. The tests were carried out at room temperature. The magnetic heating experiments were conducted by changing variable output currents ranging from 150 to 300 A. Then, 50 ml Fe-B FF and Fe-Ni-B FF at 5 wt% were studied. The experimental conditions are as described previously [26]. The work frequency of the induction heater in our experiment was 90 kHz. The work frequency is 50–100 kHz, which is safe for biomedical applications [51].

The magnetic heating results are shown in Fig. 8b, c. The temperatures of both Fe-B FF in Fig. 8b and Fe-Ni-B FF in Fig. 8c increased markedly with time. The temperature increased with increasing electrical output currents. The temperatures of the FFs under different output currents were recorded at 2000 s (in Table 2). When the electrical output current was

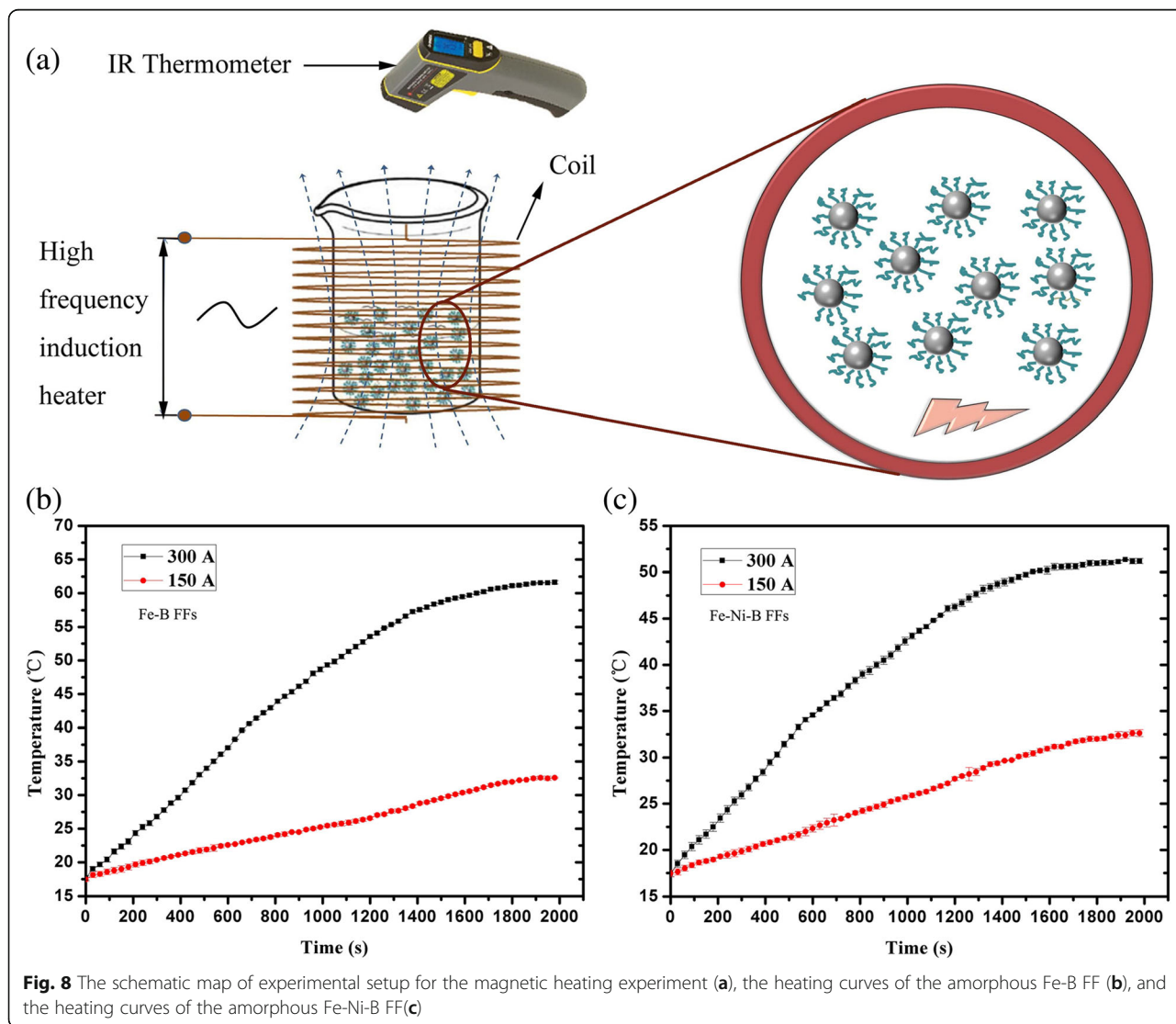


Table. 2 The temperatures of FFs in 2000 s under different output currents

FFs	T-150 A (°C)	T-300 A (°C)
Fe-B amorphous FF	32.5	61.6
Fe-Ni-B amorphous FF	32.6	51.2
$(T_{\text{Fe-B}} - T_{\text{Fe-Ni-B}}) / T_{\text{Fe-Ni-B}}$	–	20.3%

controlled at 150 A, the temperature could rise to 32.5 °C for Fe-B FF and to 32.6 °C for Fe-Ni-B FF. When the output current was 300 A, the final stable temperature was 61.6 °C and 51.2 °C for Fe-B FF and Fe-Ni-B FF, respectively. The heating efficiency of the hyperthermia effect of Fe-B FF is about 20.3% higher than that of Fe-Ni-B FF (Table 2). The hyperthermia results indicate that when the electrical current was controlled at 300 A, the temperature of Fe-B FF and Fe-Ni-B FF could raise to 42 °C in 750 s and 960 s, respectively. The specific absorption rates (SARs) could be calculated from the field assisted heating curves [52, 53]. The specific heat capacity and density of water in our paper were considered as 4.18 J g⁻¹ K⁻¹ and 1 g/cc, respectively. The SAR values were 21.91 W/g for Fe-B FF and 19.48 W/g for Fe-Ni-B FF, respectively. The SAR values were 76.15 W/g and 69.97 W/g for Fe-B FF and Fe-Ni-B FF, respectively, when the output current was 300 A. The heating experiments demonstrate that the intensity of alternating magnetic fields induced by electrical currents affect the hyperthermia of the amorphous FFs. The heating could be controlled effectively by adjusting the output current.

The heating effects of aqueous FFs are mainly attributed to Neel relaxation (magnetic dipole rotates within the particle) and Brownian relaxation mechanism (particle rotation against the hydrodynamic resistance of the carrier fluid) [54–56]. Based on the domain theory, the critical diameters of single domain are 19.6 nm, 19.2 nm, and 42.4 nm for Fe, Co, and Ni nanoparticles, respectively [57]. Here, we assume that the Fe-B amorphous nanoparticles and Fe-Ni-B amorphous nanoparticles should possess single domain structures. The magnetic spins align randomly under no external fields due to the thermal energy. When an AC field is applied, the single domain changes its magnetization orientation in response to the AC fields, and the magnetic energy is simultaneously converted into thermal energy. We conclude that the Fe-B amorphous FF and Fe-Ni-B amorphous FF have significant heating effects suggesting that Fe-B amorphous FF and Fe-Ni-B amorphous FF have a promising future for hyperthermia treatment.

Conclusions

Magnetic Fe-B, Fe-Ni-B, and Co-B amorphous nanoparticles as well as the corresponding amorphous FFs

were successfully synthesized. The nanoparticles are homogenous with amorphous structures. The shape of the amorphous particles is regular. The Fe-B, Fe-Ni-B, and Co-B amorphous nanoparticles show superparamagnetic. The Ms of Fe-B and Fe-Ni-B amorphous nanoparticles are 75 emu/g and 51 emu/g. This is approximately 2.8 and 1.9 times larger than Co-B nanoparticles, respectively. The amorphous FFs have a strong response to an external magnetic field. The yield stress increases with increasing magnetic field. The hyperthermia results indicate that when alternating electrical output current is controlled at 300 A, the temperature of Fe-B FFs and Fe-Ni-B FFs could rise to 42 °C in 750 s and 960 s, respectively. The final stable temperature was 62 °C for Fe-B FFs. The heating efficiencies of amorphous FFs demonstrate that Fe-based amorphous FFs have great potential for biomedical applications. Indeed, studies on the magnetoviscous properties of amorphous FFs and the mechanism of hyperthermia effect for amorphous FFs remains unclear and will stimulate future work.

Abbreviations

AGM: Alternating gradient force magnetometer; DSC: Differential scanning calorimeter; FFs: Ferrofluids; MFH: Magnetic fluid hyperthermia; Ms: Saturation magnetization; SAR: Specific absorption rate; TEM: Transmission electron microscopy; XRD: X-ray diffraction

Funding

Funding for the study was received from the National Natural Science Foundation of China (Grant no.51571130), Hebei Province Foundation for Returnees (Grant no.C201804) and Scientific Research Foundation for Ph.D. of Hebei GEO University (Grant no. BQ2018015).

Availability of Data and Materials

All data supporting the conclusions of this article are included within the article.

Authors' Contributions

CCY and XFB conceived and designed the experiments; CCY and MCY performed the experiments; SCZ analyzed the data; YT contributed analysis tools; CCY wrote the paper. All authors read and approved the final manuscript.

Competing Interests

The authors declare that they have no competing interests.

Publisher's Note

Springer Nature remains neutral with regard to jurisdictional claims in published maps and institutional affiliations.

Received: 13 May 2018 Accepted: 7 November 2018

Published online: 23 November 2018

References

- Rosensweig RE (1985) *Ferrohydrodynamics*. Cambridge University Press, New York
- Dickstein AJ, Erramilli S, Goldstein RE et al (1993) Labyrinthine pattern formation in magnetic fluids [J]. *Science* 261(5124):1012–1015
- Bacri J-C, Perzynski R, Shliomis MI et al (1995) "Negative-viscosity" effect in a magnetic fluid [J]. *Phys Rev Lett* 75(11):2128–2131
- Odenbach S (2002) *Ferrofluids: magnetically controllable fluids and their applications*. Springer, Heidelberg

5. Clark NA (2013) Soft-matter physics: Ferromagnetic ferrofluids [J]. *Nature* 504(7479):229–230
6. Li Z, Yao J, Li D (2016) Research on the rheological properties of a perfluoropolyether based ferrofluid [J]. *J Magn Magn Mater* 424:33–38
7. Sheikholeslami M, Shehzad SA (2017) Thermal radiation of ferrofluid in existence of Lorentz forces considering variable viscosity [J]. *Int J Heat Mass Tran* 109:82–92
8. Zakinyan AR, Dikansky YI (2017) Effect of microdrops deformation on electrical and rheological properties of magnetic fluid emulsion [J]. *J Magn Magn Mater* 431:103–106
9. Khairul MA, Doroodchi E, Azizian R et al (2017) Advanced applications of tunable ferrofluids in energy systems and energy harvesters: a critical review [J]. *Energy Convers Manage* 149:660–674
10. Shokrollahi H (2013) Structure, synthetic methods, magnetic properties and biomedical applications of ferrofluids [J]. *Mat Sci Eng C* 33(5):2476
11. Oh JK, Park JM (2011) Iron oxide-based superparamagnetic polymeric nanomaterials: design, preparation, and biomedical application [J]. *Prog Polym Sci* 36:168–189
12. Davudabadi Farahani M, Shemirani F, Gharehbaghi M (2013) Ferrofluid-based dispersive solid phase extraction of palladium [J]. *Talanta* 109:121
13. Ferroudj N, Nzimoto J, Davidson A et al (2013) Maghemite nanoparticles and maghemite/silica nanocomposite microspheres as magnetic Fenton catalysts for the removal of water pollutants [J]. *Appl Catal B-Environ* 136:9–18
14. Cheng B, Yuan L, Zhu W et al (2017) A coaxial cable magnetic field sensor based on ferrofluid filled Fabry-Perot interferometer structure [J]. *Sensor Actuat A-Phys* 257:194–197
15. Odenbach S (2002) Magnetoviscous effects in ferrofluids. Springer, Heidelberg
16. Zubarev AY et al (2005) Towards a theory of dynamical properties of polydisperse magnetic fluids: effect of chain-like aggregates [J]. *Physica A* 358:475–491
17. Zubarev AY, Iskakova LY (2004) To the theory of rheological properties of ferrofluids: influence of drop-like aggregates [J]. *Physica A* 343:65–80
18. Rajnak M, Timko M, Kopcansky P et al (2017) Structure and viscosity of a transformer oil-based ferrofluid under an external electric field [J]. *J Magn Magn Mater* 431:99–102
19. Nowak J, Borin D, Haefner S et al (2017) Magnetoviscous effect in ferrofluids diluted with sheep blood [J]. *J Magn Magn Mater* 442:383–390
20. Borin DY, Korolev VV, Ramazanov AG et al (2016) Magnetoviscous effect in ferrofluids with different dispersion media [J]. *J Magn Magn Mater* 416:110–116
21. Ryan C (2013) Sekol, et al, bulk metallic glass micro fuel cell [J]. *Small* 9:2081
22. Sundeep M, Sekol RC, Carmo M et al (2013) Metallic-glass nanostructures: tunable hierarchical metallic-glass nanostructures [J]. *Adv Funct Mater* 23(21):2708–2713
23. Zberg B, Uggowitzer PJ, Löffler JF (2009) MgZnCa glasses without clinically observable hydrogen evolution for biodegradable implants. *Nat Mater* 8:887
24. Zheng RX, Yang H, Liu T et al (2014) Microstructure and mechanical properties of aluminum alloy matrix composites reinforced with Fe-based metallic glass particles [J]. *Mater Design* 53:512
25. Stoian G, Chiriac H (2010) Magnetic properties of CoFeSiB powders, suspensions, and in rigid matrix [J]. *IEEE T. Magn* 46:495–497
26. Yang CC, Bian XF, Qin JY et al (2015) Fabrication and hyperthermia effect of magnetic functional fluids based on amorphous particles [J]. *Appl Surf Sci* 330:216–220
27. Yu MC, Yang CC, Bian XF et al (2016) Application of Fe₇₈Si₉B₁₃ amorphous particles in magnetorheological fluids [J]. *RSC Adv* 6:22511–22518
28. Wang TQ, Bian XF, Yang CC et al (2017) Ferrofluids based on Co-Fe-Si-B amorphous nanoparticles [J]. *Appl Surf Sci* 399:663–669
29. Zhao SC, Bian XF, Yang CC et al (2018) Synthesis of FeCoB amorphous nanoparticles and application in ferrofluids [J]. *Appl Surf Sci* 435:1314–1321
30. Kandasamy G, Sudame A, Bhati P et al (2017) Systematic magnetic fluid hyperthermia studies of carboxyl functionalized hydrophilic superparamagnetic iron oxide nanoparticles based ferrofluids [J]. *J Colloid Interf Sci* 514:534
31. Lahiri BB, Ranoo S, Philip J (2017) Magnetic hyperthermia study in water based magnetic fluids containing TMAOH coated Fe₃O₄ using infrared thermography [J]. *Interared Phys Techn* 80:71–82
32. Diamantopoulos G, Basina G, Tzitzios V et al (2013) Magnetic hyperthermia of laponite based ferrofluid [J]. *J Magn Magn Mater* 336(336):71–74
33. Zayed MA, Ahmed MA, Imam NG et al (2016) Preparation and structure characterization of hematite/magnetite ferro-fluid nanocomposites for hyperthermia purposes [J]. *J Mol Liq* 222:895–905
34. Lahiri BB, Muthukumar T, Philip J (2016) Magnetic hyperthermia in phosphate coated iron oxide nanofluids [J]. *J Magn Magn Mater* 407:101–113
35. Kandasamy G, Sudame A, Bhati P et al (2017) Systematic magnetic fluid hyperthermia studies of carboxyl functionalized hydrophilic superparamagnetic iron oxide nanoparticles based ferrofluid [J]. *J Colloid Interf Sci* 514:534
36. Lahiri BB, Ranoo S, Philip J (2018) Effect of orientational ordering of magnetic nanoemulsions immobilized in agar gel on magnetic hyperthermia [J]. *J Magn Magn Mater* 451:254–268
37. Guibert C, Fresnais J, Peyre V et al (2017) Magnetic fluid hyperthermia probed by both calorimetric and dynamic hysteresis measurements [J]. *J Magn Magn Mater* 421:384–392
38. Lahiri BB, Ranoo S, Philip J (2016) Infrared thermography based magnetic hyperthermia study in Fe₃O₄ based magnetic fluids [J]. *Infrared Phys Techn* 78:173–184
39. Zubarev AY, Iskakova LY, Abu-Bakr AF (2015) Effect of interparticle interaction on magnetic hyperthermia in ferrofluids [J]. *Physica A* 438:487–492
40. Yang XY, Yang B, Li XP et al (2015) Structural-controlled chemical synthesis of nanosized amorphous Fe particles and their improved performances [J]. *J Alloy and Compd* 651(6):551–556
41. Hosseini SM et al (2010) Rheological properties of a γ -Fe₂O₃ paraffin-based ferrofluid [J]. *J Magn Magn Mater* 322:3792–3796
42. Krutikova E, Ivanov AO (2010) The role of van der Waals forces in ferrofluid phase separation [J]. *Phys Procedia* 9:49–53
43. Zubarev AY, Iskakova LY (2005) Condensation phase transitions in bidisperse colloids [J]. *Physica A* 349:1–10
44. Odenbach S, Raj K (2000) The influence of large particles and agglomerates on the magnetoviscous effect in ferrofluids [J]. *Magnetohydrodynamics* 36:312–319
45. Odenbach S, Stork H (1998) Shear dependence of field-induced contributions to the viscosity of magnetic fluids at low shear rates [J]. *J Magn Magn Mater* 183:188–194
46. Odenbach S (2003) Ferrofluids-magnetically controlled suspensions [J]. *Colloid Surface A* 217:171–178
47. Dong XF, Tong Y, Ma N et al (2015) Properties of cobalt nanofiber-based magnetorheological fluids [J]. *RSC Adv* 5:13958–13963
48. Pandey BK, Shahi AK, Gopal R (2015) Magnetic colloid by PLA: optical, magnetic and thermal transport properties [J]. *Appl Surf Sci* 347:461–470
49. Inukai A, Sakamoto N, Aono H et al (2011) Synthesis and hyperthermia property of hydroxyapatite–ferrite hybrid particles by ultrasonic spray pyrolysis [J]. *J Magn Magn Mater* 323(7):965
50. Shete PB, Patil RM, Thorat ND et al (2014) Magnetic chitosan nanocomposite for hyperthermia therapy application: preparation, characterization and in vitro experiments [J]. *Appl Surf Sci* 288(2):149–157
51. Minamimura T, Sato H, Kasaoka S et al (2000) Tumor regression by inductive hyperthermia combined with hepatic embolization using dextran magnetite-incorporated microspheres in rats [J]. *Int. J. Oncol* 16:1153–1158 <https://doi.org/10.3892/ijco.16.6.1153>
52. Lahiri BB, Ranoo S, Philip J (2017) Uncertainties in the estimation of specific absorption rate during radiofrequency alternating magnetic field induced non-adiabatic heating of ferrofluids [J]. *J Phys D Appl Phys* 50(45):455005
53. Lahiri BB, Ranoo S, Philip J (2017) Magnetic hyperthermia in magnetic nanoemulsions: effects of polydispersity, particle concentration and medium viscosity. *J Magn Magn Mater* 441:310–327
54. de la Presa P, Luengo Y, Multigner M et al (2012) Study of heating efficiency as a function of concentration, size, and applied field in γ -Fe₂O₃ nanoparticles [J]. *J Phys Chem C* 116:25602–25610
55. Cervadoro A, Giverso C, Pande R et al (2013) Design maps for the hyperthermic treatment of tumors with superparamagnetic nanoparticles [J]. *PLoS One* 8:e57332
56. Bakoglidis KD, Simeonidis K, Sakellari D et al (2012) Size dependent mechanisms in AC magnetic hyperthermia response of iron-oxide nanoparticles [J]. *IEEE Trans Magn* 48:1320–1323
57. Gong W, Li H, Zhao Z, Chen J (1991) Ultrafine particles of Fe, Co, and Ni ferromagnetic metals [J]. *J Appl Phys* 69(8):5119–5121